RESEARCH ARTICLE

Novel ultrashort self-assembling peptide bioinks for 3D culture of muscle myoblast cells

Wafaa Arab[1], Sakandar Rauf[1], Ohoud Al-Harbi[2], Charlotte A. E. Hauser[1*]

[1] Laboratory for Nanomedicine, Division of Biological and Environmental Science and Engineering, King Abdullah University of Science and Technology, Thuwal, Saudi Arabia

[2] Electron Microscopy, Imaging and Characterization Core Lab, King Abdullah University of Science and Technology, Thuwal, KSA

Abstract: The ability of skeletal muscle to self-repair after a traumatic injury, tumor ablation, or muscular disease is slow and limited, and the capacity of skeletal muscle to self-regenerate declines steeply with age. Tissue engineering of functional skeletal muscle using 3D bioprinting technology is promising for creating tissue constructs that repair and promote regeneration of damaged tissue. Hydrogel scaffolds used as biomaterials for skeletal muscle tissue engineering can provide chemical, physical and mechanical cues to the cells in three dimensions thus promoting regeneration. Herein, we have developed two synthetically designed novel tetramer peptide biomaterials. These peptides are self-assembling into a nanofibrous 3D network, entrapping 99.9% water and mimicking the native collagen of an extracellular matrix. Different biocompatibility assays including MTT, 3D cell viability assay, cytotoxicity assay and live-dead assay confirm the biocompatibility of these peptide hydrogels for mouse myoblast cells (C2C12). Immunofluorescence analysis of cell-laden hydrogels revealed that the proliferation of C2C12 cells was well-aligned in the peptide hydrogels compared to the alginate-gelatin control. These results indicate that these peptide hydrogels are suitable for skeletal muscle tissue engineering. Finally, we tested the printability of the peptide bioinks using a commercially available 3D bioprinter. The ability to print these hydrogels will enable future development of 3D bioprinted scaffolds containing skeletal muscle myoblasts for tissue engineering applications.

Keywords: biomaterials; bioinks; 3D cell culture; 3D scaffold; tissue engineering; skeletal muscle cells

*Correspondence to: Charlotte A. E. Hauser, Laboratory for Nanomedicine, King Abdullah University of Science and Technology, Division of Biological & Environmental Science and Engineering, 4700 Thuwal, 23955-6900, KSA; charlotte.hauser@kaust.edu.sa

Received: October 25, 2017;**Accepted:** April 17, 2018; **Published Online:** July 13, 2018

Citation: Arab W, Rauf S, Al-Harbi O, *et al.*, 2018, Novel ultrashort self-assembling peptide bioinks for 3D culture of muscle myoblast cells. *Int J Bioprint*, 4(2): 129. http://dx.doi.org/10.18063/IJB.v4i2.129

1. Introduction

Approximately half of human adult body mass is muscle tissue. Skeletal muscle tissue carries out various functions in the body such as respiration, protection of abdominal viscera, and controlling movements of limbs[1]. Muscle tissue has a native ability to regenerate/repair. However, muscle damage that is larger than a critical volume is more challenging to fix *via* natural physiological processes which causes muscle tissue loss and functional weakness[2]. Surgical intervention may be required to restore normal function and prevent scar tissue formation[3].

Clinical conditions such as tumor resection, traumatic injuries, and muscular dystrophy may result in volumetric muscle loss. These ailments affect millions of people worldwide and cause significant economic and social problems[4,5]. Autografting is the current gold standard to treat substantial skeletal muscle loss/damage. However, there are some bottleneck issues in surgical tissue grafting techniques such as donor site morbidity, loss of function at the donor site and shortage of healthy

donor tissues.

Tissue engineering is an alternative approach for volumetric muscle loss treatment and organ fabrication[6], where the use of biological scaffolds are being explored. These structures have been fabricated to deliver the aesthetic and functional needs of skeletal muscle tissue regeneration and have been tested *in vitro* and implanted in vivo to facilitate the native functions of the damaged tissue[7–9]. However, there are a few negative outcomes associated with autologous cell-laden simple scaffolds such as high complexity cell encapsulated scaffolds[10–14].

Three-dimensional bioprinting technology is a promising technique, constructing 3D structures to fabricate platforms used for tissue engineering and regenerative medicine[15,16]. The scaffold is a major component of a tissue-engineered construct that is made from biomaterials with 3D architecture. It provides a microenvironment that accommodates more cells, promotes cell adhesion and proliferation. Despite its promise, the lack of suitable bioinks has constrained the development of bioprinting technologies. Biocompatibility, biodegradability, non-immunogenic, non-mutagenic and non-hemolytic scaffolds are essential properties for the long-term culture of cells and engineered tissue for implantation to avoid adverse physiological side effects. Several biomaterials have been used *in vitro* as bioinks[17,18]. Scaffolds from self-assembling peptides are of particular interest for bioprinting due to their synthetic but natural background. They have been used as biomaterials for applications in regenerative medicine and as matrices for the delivery of encapsulated bioactive molecules for therapeutic applications[18-22]. The peptide scaffolds were used in injectable forms enabling more accurate and localized delivery of cancer drugs which in turn helped to reduce harsh side effects generally associated with cancer treatments[23]. Ultrashort amphiphilic peptides also showed accelerated skin regeneration when used a burn wound dressings[24].

Scaffolds aimed for skeletal muscle tissue engineering must be capable of accommodating more cells and promoting the formation of highly aligned myofibers throughout the construct[25-28]. Porous scaffolds with aligned morphology in 3D, micro/nanofibrous structures have been studied for skeletal muscle tissue engineering[29]. It is imperative for a successful skeletal muscle platform to present the right kind of structural cues to pre-align muscle cells to enhance myogenic differentiation and myotube formation[30,31]. Many hydrogels have been used and evaluated for their cellular activity, mechanical properties, and myogenic potential. There is still need to find the most appropriate material which has the efficacy to maintain mechanical stability and promote myotube formation[32]. The 3D network of short self-assembled peptides nanofibrous hydrogels has shown to support pluripotent stem cells survival and differentiation[33]. Herein, we have tested the biocompatibility of two different tetramer self-assembling peptides for 3D cell culture of mouse myoblast (C2C12) to validate the effectiveness of these peptide bioinks for long-term cell viability in 3D. We found that the 3D cultured cells within the hydrogels preserve cells viability and promote growth and alignment of mouse myoblast cells. Moreover, 3D cultured cells using our scaffold start replacing the degrading hydrogel by secreting their matrix. We also tested the printability of these peptide bioinks by using a commercially available 3D bioprinter. We propose that these peptide bioinks could be promising biomaterials for 3D bioprinting and tissue engineering applications.

2. Materials and Methods

Two tetramer self-assembling peptides CH-01 and CH-02 were procured from Bachem AG, (Budendorf, Switzerland). Mouse myoblast cells (C2C12) were purchased from (ATCC, USA). Dulbecco's Modified Eagle Medium (DMEM), fetal bovine serum (FBS), Dulbecco's phosphate-buffered saline (PBS) solution, and penicillin-streptomycin antibiotics (P/S) were purchased from Gibco (Grand Island, USA). CellTiter-Glo® Luminescent 3D cell viability assay kit was procured from Promega (Madison, USA). MTT Cell Proliferation Assay kit, Cytotoxicity assay kit (CytoTox96) and LIVE/DEAD® Viability/Cytotoxicity Kit were purchased from ThermoFisher Scientific, USA, Promega, USA and Life TechnologiesTM, USA, respectively. Immunostaining antibodies anti-vinculin and Rhodamine-Phalloidin were purchased from (Invitrogen, USA), and anti-mouse IgG-FITC was purchased from Sigma, USA. T175 or T75 cell culture flasks and 96-well plates were procured from Corning, USA.

2.1 Hydrogel Preparation

Two tetramer peptides CH-01 and CH-02 were used in this study. Peptides were synthesized by Bachem AG, (Budendorf, Switzerland) using solid phase peptide synthesis and purified to above 95% *via* HPLC. Lyophilized peptide powder was dissolved in Milli-Q water and vortexed to get a homogenous solution. Subsequently, 10× phosphate buffered saline at the final concentration of 1× was added to the peptide solution and vortexed briefly. Gelation occurred within a few seconds in CH-01 at 4 mg/mL and CH-02 at 3 mg/mL peptide concentration. Alginate-gelatin was used as a positive control.

Alginate-gelatin was prepared by mixing an equal amount (1:1) of each content; then serial dilution

was made from the stock solution. Briefly, gelatin (porcine skin type A, Sigma) was dissolved at 30 mg/mL in Milli-Q water under constant stirring at 40 °C, then autoclaved. After that, 30 mg/mL of Alginic acid sodium salt powder (Sigma) was dissolved in the gelatin solution. The resultant alginate-gelatin solution was then ionically crosslinked by calcium chloride ($CaCl_2$, 150 mM, Sigma) for 5 min. Finally, calcium chloride was removed and corsslinked alginate-gelatin was washed with phosphate buffer saline.

2.2 Scanning Electron Microscopy Analysis

The hydrogels were dehydrated using gradient ethanol: 30, 50, 70, 90 and 100% was used for dehydration, each step for 15 min. Further dehydration was done twice in 100% ethanol for 15 min each. The dehydrated samples were dried for 20 min in 1:2 solution of hexamethyldisilazane (HMDS): 100% ethanol, followed by 20 min incubation in a fresh solution of 2:1 HMDS:100% ethanol and then 20 min in 100% HMDS; the last step was repeated twice. Finally, the samples were left in a fume hood overnight with the container cap left loose. The samples were mounted onto sample holders using conductive tape, and then sputter-coated with Iridium 5 nm and Gold/Palladium 3 nm. The coated samples were then examined with field emission scanning electron microscopy system (FEI Nova Nano630 SEM, Oregon, USA).

2.3 Cell Culture

Mouse myoblast cells (C2C12) were cultured either in a T175 or T75 culture flask in complete DMEM media (10% fetal bovine serum, and 1% penicillin/streptomycin). The cells were incubated in a humidified incubator with 95% air and 5% CO2 at 37 °C. The cells were subcultured by trypsin at approximately 80% confluence. The culture media was replenished every 48 h.

2.4 3D Culture of Myoblast Cells in Peptide Hydrogels

Mouse myoblast cells were encapsulated in peptide hydrogels in glass bottom dish (Nunc, 12 mm). Peptide solutions CH-01 (4 mg/mL) and CH-02 (3 mg/mL) were added to the plate at 40 µL/dish. Mouse myoblast cells (30,000 cells/dish) that re-suspended in 2× PBS were gently mixed with peptide solutions. Gelation occurred within 3–5 min, and subsequently, the culture medium was added to the dishes. On day 2, 4 and 8, the 3D cell viability assay, live/dead assay and cytoskeletal staining were performed.

2.5 Biocompatibility Studies

2.5.1 MTT Assay

Biocompatibility studies were carried out in 96-well plates. C2C12 were seeded at a density of 10,000 cells/well and incubated overnight in the complete growth medium. The cell culture medium was replenished, and different concentrations of peptide solution were added to the wells. The wells without peptides were used as positive control. After 24 h incubation at 37 °C, a colorimetric MTT assay was performed to determine cell viability according to the manufacturer's protocol. Briefly, 10% MTT reagent was mixed with fresh serum-free medium and added to each well including positive control wells. The plate was incubated at 37 °C between 2–4 h, then, 100 µL of DMSO was added to each well to dissolve the insoluble crystals of formazan. Finally, a plate reader (PHERAstar FS, Germany) was used to read the absorption of individual wells at 540 nm.

2.5.2 Cytotoxic Assay

Mouse myoblast cells were seeded and treated with peptides according to the protocol described above. After 24 h incubation, 50 µL from the incubated medium with a different concentration of peptides and alginate-gelatin were transferred to a new 96-well plate followed by adding 50 µL of cytotoxic reagent and incubated for 30 min in the dark. Stop solution was added, and the release of lactate dehydrogenase (LDH) was quantified at 490 nm using a plate reader (PHERAstar FS, Germany).

2.5.3 3D Cell Proliferation Assay

CellTiter-Glo® Luminescent 3D cell viability assay was performed to quantify ATP production in 3D hydrogels which reflect the number of metabolically active cells. After each time point, an equal amount of CellTiter-Glo® luminescent reagent was added to the 3D cultured hydrogels and mixed for 2 min to digest the hydrogels and then incubated for 25 min. Finally, the luminescence was recorded using a plate reader (PHERAstar FS, Germany).

2.5.4 Live/Dead Staining

Live/Dead fluorescence staining is a standard fluorescence imaging method used to visualize live cells (green) and dead cells (red). After each time point, the cell culture media was removed and incubated for 30 min in the dark in DPBS solution containing live/dead fluorescence staining (2 µM calcine for live cells (green) and 4 µM ethidium homodimer-1 for dead cells (red). Finally, the staining solution was removed and washed with fresh DPBS[33]. An inverted confocal microscope (Zeiss LSM 710, Germany) was used to observe and image the live and dead cells.

2.5.5 Cytoskeletal Staining

The morphology of mouse myoblast cells was studied at each time point using immunofluorescence staining. In brief, the cells were fixed in 4% paraformaldehyde for 30 min. After the incubation, the cells were washed three times using DPBS. The cell membrane was permeabilized by incubating for 10 min in ice-cold permeabilization buffer (300 mM sucrose, 3 mM $MgCl_2$, and 0.5% Triton X-100 in PBS solution). This solution was replaced with blocking buffer solution (5% FBS, 0.1% Tween-20, and 0.02% sodium azide in PBS) for 30 min. The permeabilized cells were then stained with anti-vinculin (1:300) for 1 h, then with anti-mouse IgG-FITC and rhodamine-phalloidin (1:300) for 1 h at 37 °C. After that, DAPI staining (1:100 water) was used to stain the nucleus for 5 min[33]. Fluorescence confocal microscopy (Zeiss LSM 710 Inverted Confocal Microscope, Germany) was used to observe the cell morphology.

2.5.6 Analysis of Myoblast Alignment

The alignment of myoblast cells within different scaffolds was determined using Fast Fourier transform (FFT) of fluorescence confocal image which shows the summation of pixel intensities in radial coordinates around the origin. The two-dimensional alignment plot was obtained using ImageJ software supported by an oval profile plug-in. Briefly, the color images were converted into grayscale images. Then, the FFT was applied to the grayscale images by placing circular projection on the FFT images. The summation of pixel intensities was measured along the radius of the circular projection for each angle (0 to 180°) using ImageJ oval profile plug-in. A two dimensional FFT alignment plot was produced by plotting the pixel intensities against the corresponding angle of acquisition. The degree of cells alignment was quantified through the shape and the height of the peaks[34]. The degree of alignment is indicated by a high and narrow peak whereas a broader peak means that more than one axis of alignment may be present. A random alignment will result in no distinguishable peak in the alignment plot[34,35].

2.6 Printability of Peptide Hydrogels

A commercially available extrusion-based 3D bioprinter was used to test the printability of peptide bioinks. The 3D bioprinter used has two extrusion printing heads that can print two different bioinks. The peptide bioink CH-02 (20 mg/mL in water) was loaded into a 3 mL cartridge and fitted onto one of the extrusion head of the printer. The extrusion head was connected to an external air supply source with a manual pressure regulator to extrude peptide bioink from the cartridge. A highly viscous solution of the peptide (20 mg/mL) bioink CH-02 was used so that it can be extruded from the printing nozzle. In case of lower concentrations of peptides (3 mg/mL or 4 mg/mL), we were unable to print due to the low viscosity of the peptides at these concentrations. Two different structures circle (8 mm diameter) and square (6 × 6 mm^2) were printed in a layer-by-layer fashion. The nozzle diameter was 400 µm, and an air pressure of 12 KPa with a printing speed of 4 mm/sec was used for the peptide printing. Finally, 2× PBS buffer was added on top of the ring or square structure to form the peptide hydrogel.

2.7 Statistical Analysis

All the results are presented as a mean ± SD. Three similar experiments were performed independently for each type of test. One-way analysis of variance determined statistical differences among the experimental groups. When the *P*-values were $P < 0.05$, the results were considered to be statistically significant.

3. 3. Results

3.1 SEM Analysis of Peptide Hydrogels

The nanofibrous morphology of self-assembling peptides was evaluated using SEM and compared to those observed in bovine collagen (Figure 1A, B, C) which comprises a unique triple-helical structure[36]. SEM results confirmed that both CH-01 (Figure 1D, E, F) and CH-02 (Figure 1G, H, I) peptide hydrogels form a nanofibrous network. The detailed assessment of CH-01 (Figure 1D, E, F) and CH-02 (Figure 1G, H, I) showed that the fibrous structures of these peptides resemble the fibrous structure of collagen in terms of architecture.

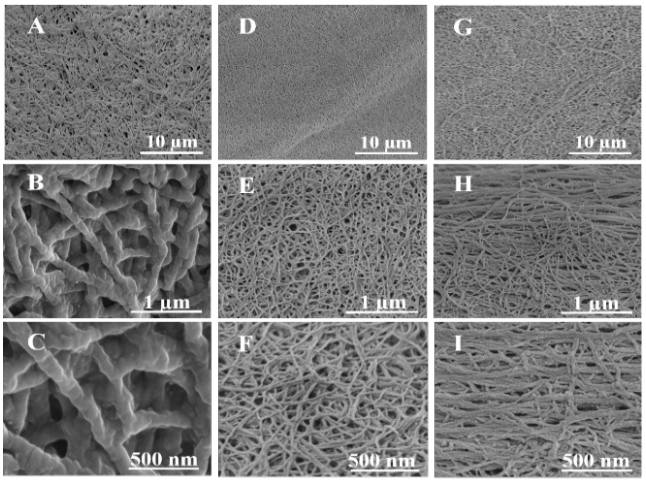

Figure 1. Ultrashort peptides self-assemble into three-dimensional nanofibrous networks. Field emission scanning electron microscopy images of 2.5 mg/mL bovine collage type I (**A, B, C**), 4 mg/mL CH-01 (**D, E, F**) and 3 mg/mL CH-02 (**G, H, I**).

3.2 Biocompatibility Studies

3.2.1 Cell Viability Results (MTT Assay)

The biocompatibility of both peptides was evaluated by testing cell proliferation after 24-h incubation with different peptide concentrations. Alginate-gelatin was used as a positive control (Figure 2A). The number of viable cells was quantified using the MTT assay. A standard curve for a known number of cells was plotted to quantify the number of viable cells (Figure 2B). The test results indicated that there was a significant difference in cell proliferation between the peptides and alginate-gelatin as compared to the cell grown on tissue culture plate (TCP) without the addition of these biomaterials. This may be due to the nutrients depletion to the cells caused by the higher amounts of the peptide or alginate-gelatin biomaterials. Peptide bioinks CH-01 and CH-02 forms stable hydrogels at 4 mg/mL and 3 mg/mL respectively as compared to 30 mg/mL of alginate-gelatin bioink. The cell proliferation was significantly decreased in the concentrations of alginate-gelatin required to produce alginate-gelatin hydrogel (30 mg/mL) when compared to both peptides (Figure 2).

3.2.2 Peptides Cytotoxicity

Cell mortality was assessed by measuring the LDH release into the culture medium after 24 h incubation with different concentrations of both peptides. Our results revealed that there was no significant cytotoxicity induced by the peptide hydrogels (Figures 3B and C) compared to alginate-gelatin (Figure 3A).

3.2.3 Cell proliferation and ATP Production in 3D Hydrogels

CellTiter-Glo® Luminescent 3D cell viability assay was performed to quantitatively evaluate the potential of peptide hydrogels to support the spread of C2C12 cells in the 3D culture hydrogel. This test was conducted to check the biocompatibility of peptide hydrogels at CH-01 (4 mg/mL) and CH-02 (3 mg/mL). This test is based on the luminescence detection of the amount of ATP production which is correlated to the number of viable cells. This 3D assay result showed a time-dependent increase in cell proliferation of the peptide hydrogels (Figure 4). After day 2, the cell numbers were comparable between the CH-01, CH-02, and alginate-gelatin in 3D-culture. However, after day 4, the cell proliferation is significantly higher in CH-01 and CH-02 than alginate-gelatin. It is worth mentioning that on day 8, the cell proliferation was comparable between the peptide hydrogels and the control. In addition to this, the cell number in CH-01 were higher when compared to CH-02 and alginate-gelatin.

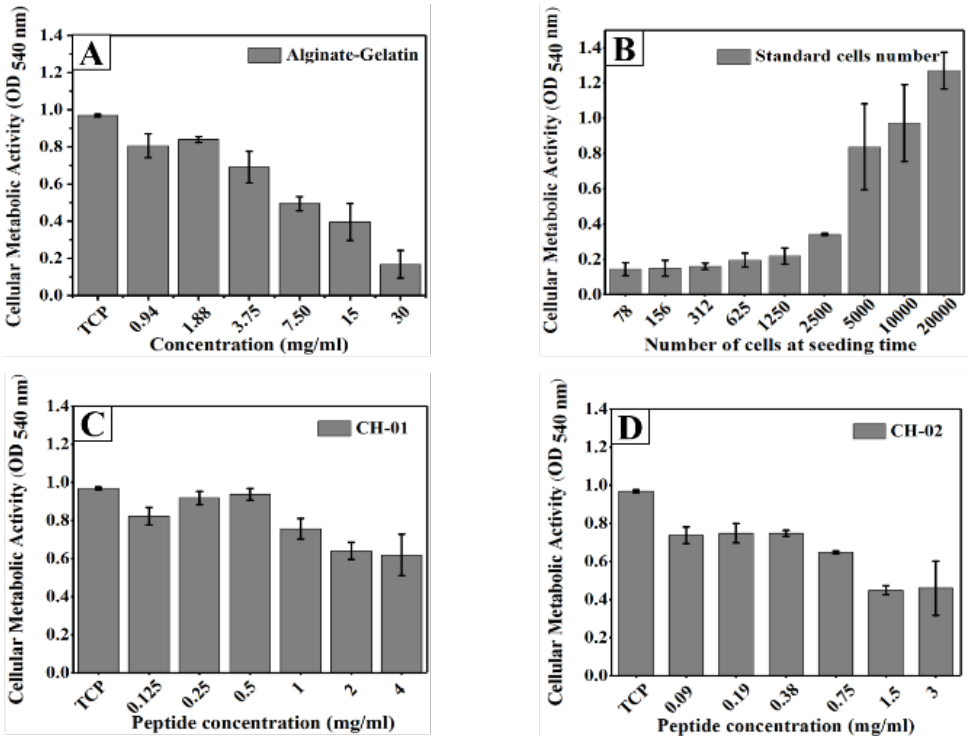

Figure 2. Graphical representation of MTT assay of mouse myoblast cells incubated with different peptide concentrations for 24 h. Alginate-Gelatin (1:1) was used as positive control (**A**), CH-01(**C**), CH-02 (**D**) and a standard curve for a known number.

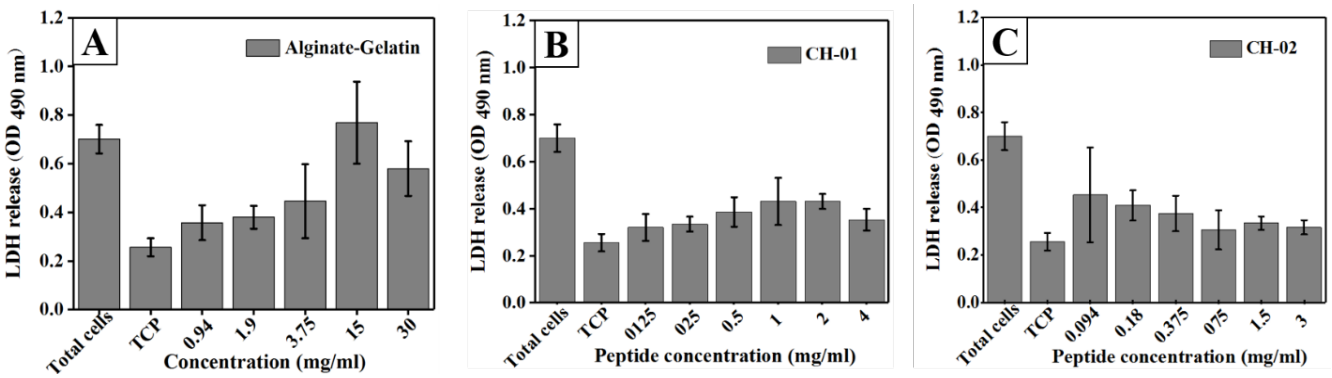

Figure 3. Representation of cytotoxicity on mouse myoblast cells after 24 h incubation with different peptide concentrations. Alginate-Gelatin used as positive control (**A**), CH-01 (**B**), and CH-02 (**C**). Error bars, mean ± S.D.

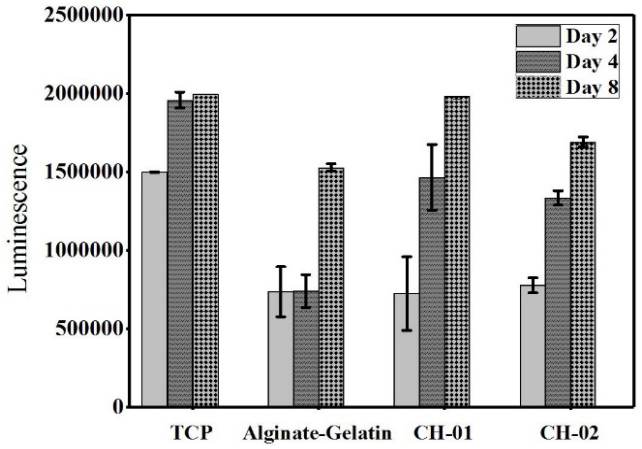

Figure 4. 3D viability assay of mouse myoblast cells encapsulated in peptide hydrogels, 4 mg/mL CH-01 and 3 mg/mL and 30 mg/mL alginate-gelatin (1:1).

3.2.4 Live/ Dead Assay Results

To further analyze the cellular compatibility of peptides, C2C12 cells were encapsulated in 4 mg/mL CH-01 and 3 mg/mL CH-02 and incubated for 2, 4 and 8 days. The biocompatibility and cytotoxicity of both peptides were tested qualitatively using live/dead staining. The intensity of green color indicated that the majority of cells were viable and that a negligible number of dead cells were observed after 2, 4 and 8 days of 3D-culture as shown in Figure 5. This result indicates the biocompatibility of our peptide hydrogels in the tested concentrations.

3.2.5 Cytoskeleton Staining of C2C12 Cells in 3D Hydrogels

Actin morphology is direct evidence to show the compatibility of hydrogels, alignment of cells in 3D scaffold and differentiation efficiency of the cells. The biocompatibility of peptide hydrogels was studied in 3D culture hydrogel after 2, 4 and 8 days (4 mg/mL of CH-01, 3 mg/mL of CH-02 and 30 mg/mL of alginate-gelatin) By staining the F-actin and nucleus of cell-laden hydrogels. After two days of culture, the F-actin filaments in C2C12 cells were well stretched and extended in all the tested condition (Figures 6B, E and H). By day 4, the F-actin was well spread, extended and distinct in CH-01 (Figure 6F) while on CH-02 (Figure 6I) and alginate-gelatin (Figure 6C) they were dense but not well pronounced. Interestingly, it was observed hat myoblasts were aligned at a particular angle in CH-01 hydrogels which could be attributed to the fact that CH-01 provides a structural cue to the myoblast cells and help to align and proliferate. On day 8, the cell alignments were comparable on all the three hydrogels. F-actin was well stretched, spread and dense in CH-01 (Figure 6G), CH-02 (Figure 6J) and alginate-gelatin (Figure 6D). This result further confirms the live/dead staining and MTT assay results.

3.2.6 Myoblast Alignment within the Scaffold

The alignment of the cells was confirmed applying the two dimensional (2D) Fast Fourier Transform (FFT) algorithm. FFT alignment plots in Figure 7 illustrated that on day 2, the myoblast cells alignment was comparable in case of both peptides and alginate-gelatin bioinks. By day 4, a high degree of myoblast alignment was observed in both CH-01 (Figure 7E) and CH-02 (Figure 7F) as compared to alginate-gelatin (Figure 7D). It is worth mentioning that the myoblast alignment on day 8 was comparable in both CH-01(Figure 7H) and CH-02 (Figure 7I). In contrast, a completely random alignment was shown in alginate-gelatin (Figure 7G) with no obvious peak in the alignment plot.

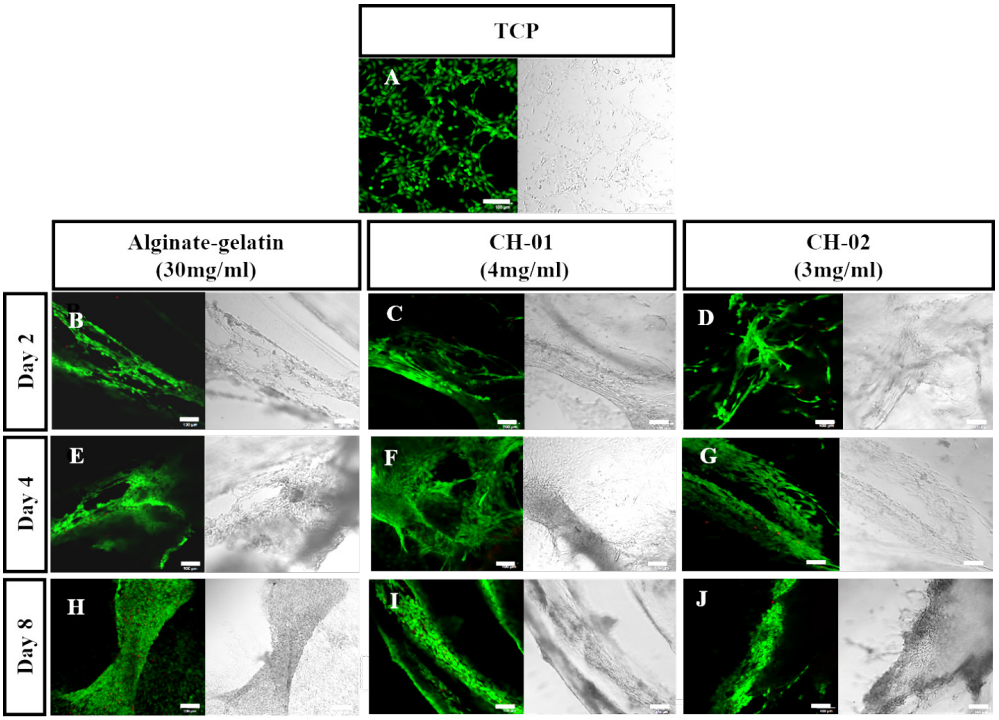

Figure 5. Live/dead staining of mouse myoblast cells encapsulated in peptide hydrogels, 4 mg/mL CH-01 and 3 mg/mL CH-02, and 30 mg/mL alginate-gelatin (1:1), for different time points. Alginate-Gelatin used as positive control (**B, E, H**), CH-01 (**C, F, I**), and CH-02 (**D, G, J**) at day 2, 4 and 8, respectively. Scale bars 100 µm.

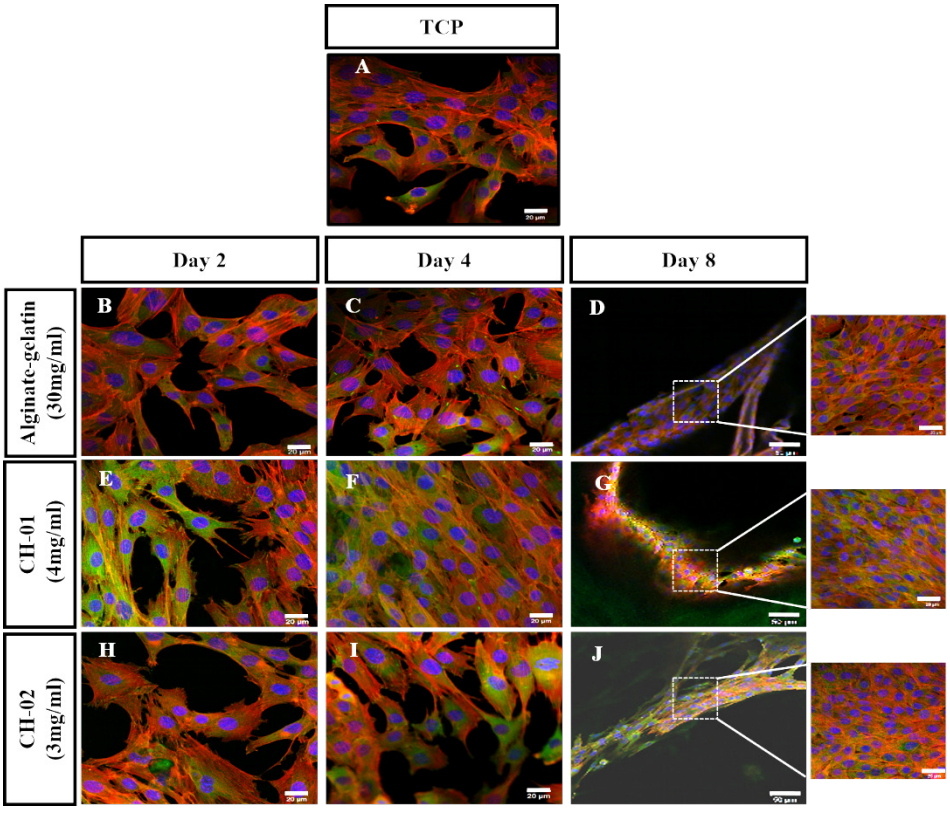

Figure 6. Overlaid confocal fluorescence images of mouse myoblast cells encapsulated in peptide (4 mg/mL CH-01 and 3 mg/mL; CH-02) and alginate-gelatin (1:1) hydrogels. The encapsulated cells were cultured for different days and finally analyzed using fluorescence confocal microscopy (Nucleus shown in blue, F-actin shown in red and vinculin in green). (**A**) Mouse myoblast cells cultured on tissue culture plate (TCP). Alginate-gelatin (**B, C, D**), CH-01 (**E, F, G**), and CH-02 (H, I, J) at day 2, 4, and 8, respectively. Scale bar is 20 µm.

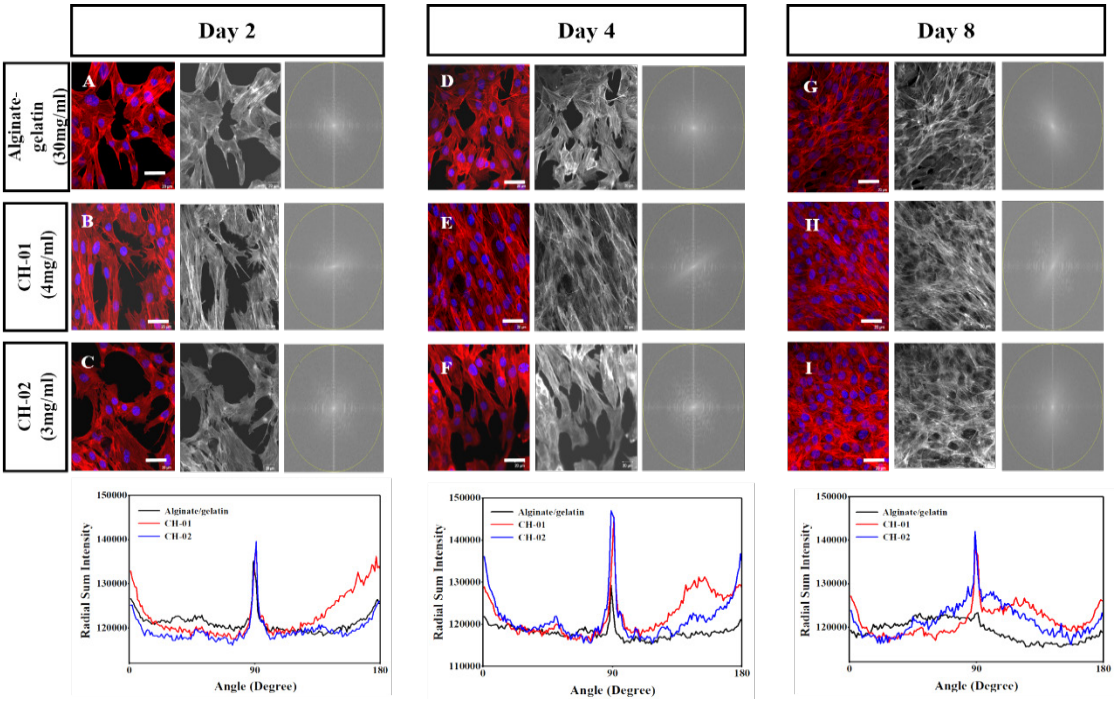

Figure 7. Quantification of C2C12 alignment within different scaffolds for different time points. Column 1 shows the fluorescent image of the Myoblast cells within different scaffold; Alginate/gelatin (**A, D, G**), CH-01 (**B, E, H**) and CH-02 (**C, F, I**) at day 2, 4 and 8, respectively. Colum 2 shows the grayscale images to perform FFT analysis. Column 3 shows the two-dimensional FFT of the grayscale images image. The bottom graphs show the FFT plot for CH-01, CH-02 and alginate-gelatin which confirm the alignment of myoblast cells after 2, 4, and 8 days, (scale bars = 20 µm).

3.3 Printability of Peptide Bioinks

Printability of peptide bioinks was verified using a commercially available 3D bioprinter. It was observed that these peptides bioinks are printable with a good shape fidelity that is essential for 3D bioprinting (Figure 8A, B). As a proof of concept, ring and square shapes were printed using the peptide bioinks. The dimensions of the printed circle were 8 mm outer diameter with 1 mm edge thickness. We used 400 µm nozzle and 3 layers to print a circle or square in a layer-by-layer fashion. The edge thickness of the circle and square was calculated to be 1 mm that means the peptide bioinks spread (600 µm) after printing and as a result, the edge thickness of the circle or square was increased as compared to the expected thickness.

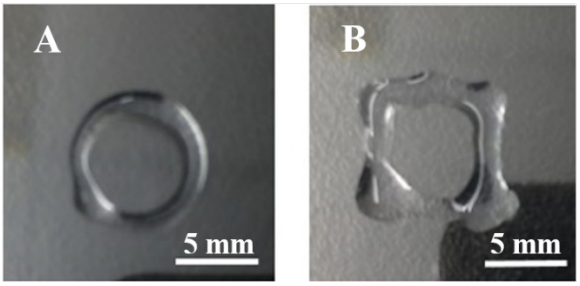

Figure 8. Bioprinting of peptide hydrogels; Bioprinted peptide hydrogel in different structures: (**A**) Circle; (**B**) Square.

4. Disscusion

Skeletal muscle tissue engineering is a promising field for diseased and injured tissue replacement and applications. Many technologies have been used to generate 3D muscle construct, but none of these methods has succeeded to mimic the gross native morphology of the tissues and organs[37–39]. On contrary, 3D bioprinting is a superior technology among several currents used techniques due to its accuracy in producing dense, cellularized construct with the advantage in producing scalable and customized tissue constructs in addition to the rapid and cost-effectivity[15,26,40]. On the other hand, lacking a proper biocompatible bio-ink with supportive mechanical properties for 3D cell culture is a major obstacle resulting in lack of cells deposition accuracy and structural organization[26,41]. Therefore, new materials with improved physical, mechanical, and chemical properties are required to improve the muscle tissue engineering applications. We have developed a novel class of ultrashort peptides that self-assemble into hydrogels.

We have developed a novel class of ultrashort peptides that self-assemble into hydrogels. We observed the formation of ECM with a high level of viable cells inside the 3D peptide hydrogels over a period of eight days. An excellent printability and shape fidelity that is essential

for 3D bioprinting was observed with both peptides. Formation of ECM with a high level of viable cells was observed with the 3D-culture cell. The formation of cell-laden, viable printed constructs was accomplished the deposition process *via* cell embedded within decellularize ECM hydrogel[42]. It has been well known that alignment of scaffold architecture plays a significant role in the proper alignment of myofibers, which in turn induce the conduction of force and contractility towards the regeneration of functional skeletal muscle[43]. Our results showed that the myoblast cells encapsulated in the peptide hydrogel scaffolds demonstrated a high level of cell viability, as well as structural stability without the requirement for chemical cross-linking. The morphology and architecture of our hydrogels are similar to that of the natural ECM as shown in the SEM micrographs. SEM results have revealed a dense fibrous mesh network with a 10–15 nm thickness of the fibers, mimicking the architecture of the microenvironments found in the ECM[35]. Recently, the clinical importance of ECM based materials in tissue-engineering are highlighted for different tissue regeneration applications[44,45]. The ECM based material enables the remodeling of construct at the damaged site and encourages the formation of a particular tissue rather than scar tissue formation[46]. Hydrogels prepared from natural polymers, such as alginate, gelatin, collagen, chitosan, *etc*., have been used for bioprinting[47–52]. Alginate is a biomaterial from brown algae and widely used in various pharmaceutical and medical applications due to its biocompatibility and low toxicity[53].

Gelatin, a hydrolyzed form of collagen, has been widely used in wound dressing, as pro-angiogenic matrices and absorbent pads for surgical applications[54–56]. Alginate-gelatin blends have been used as carriers in drug delivery[57,58] and wound dressing fibers[59]. Also, alginate-gelatin blends have been used as bioinks for 3D bioprinting applications[60-62]. In this study, we used alginate-gelatin blend bioink as a positive control. 3D cell viability results confirmed that the cells encapsulated in our hydrogels were healthy whereby the proliferation increased by day 8 and did not change the bio-reconstruction. CH-01 preserved higher cell numbers when compared to CH-02 and alginate-gelatin which could be attributed to the fact that CH-01 may be providing native cues and offers more surface area to the cells to divide and grow. Also, this peptide hydrogel has sufficient porosity to accommodate more cells and help in viability. Actin is a major cytoskeletal protein present in eukaryotic cells which gave information about cell shape and motility. This protein also has several other functions such as direct regulation of different transcription factors[63].

Immunofluorescence results of myoblast cells encapsulated in peptide scaffolds illustrated prominently well-organized actin fibers and alignment of myoblast over the scaffold. Since the reorganization of F-actin plays a crucial role in cell differentiation initiation, we concluded that our peptide hydrogels promote myoblast alignment and facilitate the synthesis of confluent myoblasts through stimulation of the adhesion proteins and cytoskeletal pattern which lead to prompt differentiation. These results do not eliminate the importance of studying the factors secretion by myoblasts and myotubes during culturing or embedded in the ECM that may also alter the scaffold stiffness[64]. Controlling the alignment of cells is critical for any tissue-engineered graft to enhance their functionality and to acquire a highly cellular organization[35]. Different cells have been proofed for their high degree of alignment including, neural cells[65], cardiac muscle[66], skeletal muscle[67], corneal tissue[68] and vascular tissue[69,70]. In particular, the alignment of skeletal muscle cells is essential to maximize the contractile power of the tissue[31]. Quantification of cellular alignment is necessary to check the effectiveness of biomaterials and the engineered microenvironment on the organization of cells. The alignment of myoblast cells was confirmed using a two dimensional fast Fourier transform (FFT) of the fluorescence images[34,35]. Our results showed that myoblast cells aligned at a particular angle in CH-01 hydrogels after four days which could be attributed to the fact that CH-01 scaffolds provide a structural cue to the myoblast cells and help to align and proliferate. However, a completely random alignment has seen in the alginate-gelatin as illustrated in the alignment plot in Figure 7. Finally, as a step towards 3D bioprinting applications of these peptide bioinks, we showed the printability of these peptides using extrusion based printing method. These results indicated that the peptide bioinks are printable and are a promising candidate for 3D bioprinting of muscle myoblasts cells to create elastic designed and accurately defined structures with a uniform distribution of cells within the construct that could lead to a better architectural organization of muscle cells for the development of skeletal muscle tissue engineering application.

5. Conclusion

Our results indicated that both peptide hydrogels offer a substantial increase in cell viability and promote cell growth and expansion of myoblast cells. Furthermore, we showed that high cell viability retained with 3D cultured constructs for at least eight days. We have also shown that both peptides are printable which opens up the possibility of 3D bioprinting of muscle myoblasts and other cell types in the future. We believe that the described results represent an advancement in the

context of engineering skeletal muscle tissue, providing the chance to rebuild missing, failing, or damaged muscles parts in the future.

Acknowledgments

We want to thank Ms. Soumaya Belkharchouche for kindly proof-reading the manuscript. The research reported in this publication was supported by funding from King Abdullah University of Science and Technology (KAUST).

Author Contributions

C.A.E.H designed and supervised the project. W.A performed the majority of the experiments and wrote the manuscript, S.R carried out the printing using the peptide bioinks and helped with editing the manuscript, and O.H took the SEM images.

Conflict of Interest and Funding

The authors declare that they do not have any competing interests.

References

1. Stilhano R S, Madrigal J L, Wong K, *et al*., 2016, Injectable alginate hydrogel for enhanced spatiotemporal control of lentivector delivery in murine skeletal muscle. *J Control Release*, 237: 42–49. http://dx.doi.org/10.1016/j.jconrel.2016.06.047
2. Chaturvedi V, Dye D E, Kinnear B F, *et al*., 2015, Interactions between skeletal muscle myoblasts and their extracellular matrix revealed by a serum free culture system. *PLO S*, 10(6): 1–27. https://dx.doi.org/10.1371/journal.pone.0127675
3. Järvinen T A H, Järvinen T L N, Kääriäinen M, *et al*., 2007, Muscle injuries: Optimising recovery. *Best Pract Res Clin Rheumatol*, 2(2): 317–331. http://dx.doi.org/10.1016/berh.2006.12.004
4. Manring H, Abreu E, Brotto N, *et al*., 2014, Novel excitation-contraction coupling related genes reveal aspects of muscle weakness beyond atrophy: New hopes for treatment of musculoskeletal diseases. *Front Physiol*, 5: 1–12. http://dx.doi:10.3389/fphys.2014.00037
5. Grasman J M, Zayas M J, Page R L, *et al*., 2015, Biomimetic scaffolds for regeneration of volumetric muscle loss in skeletal muscle injuries. *Acta Biomater*, 25: 2–15. http://dx.doi.org/10.1016/j.actbio.2015.07.038
6. Zorlutuna P, Annabi N, Camci-Unal G, *et al*., 2012, Microfabricated biomaterials for engineering 3D tissues. *Adv Mater*, 24(14): 1782–1804. https://dx.doi:10.1002/adma.201104631
7. Sato M, Ito A, Kawabe Y, *et al*., 2011, Enhanced contractile force generation by artificial skeletal muscle tissues using IGF-I gene-engineered myoblast cells. *J Biosci Bioeng*, 112(3): 273–278. http://dx.doi.org/10.1016/j.jbiosc.2011.05.007
8. Lepper C, Partridge T A, Fan C M, 2011, An absolute requirement for Pax7-positive satellite cells in acute injury-induced skeletal muscle regeneration. *Development*, 138(17): 3639–3646. http://dx.doi.org/10.1242/dev.067595
9. Kuraitis D, Giordano C, Ruel M, *et al*., 2012, Exploiting extracellular matrix-stem cell interactions: A review of natural materials for therapeutic muscle regeneration. *Biomaterials*, 33(2): 428–443. http://dx.doi.org/10.1016/j.biomaterials.2011.09.078
10. Atala A, Bauer S B, Soker S, *et al*., 2006, Tissue-engineered autologous bladders for patients needing cystoplasty. *Lancet*, 367(9518): 1241–1246.http://dx.doi:10.1016/S0140-6736(06)68438-9
11. Carsin H, Ainaud P, Le Bever H, *et al*., 2000, Cultured epithelial autografts in extensive burn coverage of severely traumatized patients: A five year single center experience with 30 patients. *Burns*, 26(4): 379–387. http://dx.doi.org/10.1016/S0305-4179(99)00143-6
12. Raya-Rivera A, Esquiliano D R, Yoo J J, *et al*., 2011, Tissue-engineered autologous urethras for patients who need reconstruction: An observational study. *Lancet*, 377(9772): 1175–1182.http://dx.doi.org/10.1016/S01406736(10)62354-9
13. Warnke P H, Springer I N, Wiltfang J, *et al*., 2004, Growth and transplantation of a custom vascularised bone graft in a man. *Lancet*, 364(9436): 766–770.http://dx.doi.org/10.1016/S01406736(04)16935-36
14. Atala A, Kasper F K, Mikos A G, 2012, Engineering complex tissues. *Sci Transl Med*, 4(160): 160 rv12. http://dx.doi.org/10.1126/scitranslmed.3004890
15. Murphy S V, Atala A, 2014, 3D bioprinting of tissues and organs. *Nat Biotechnol*, 32(8): 773–785. http://dx.doi.org/10.1038/nbt.2958
16. Derby B, 2012, Printing, and prototyping of tissues and scaffolds. *Science*, 338(6109): 921–926. http://dx.doi.org/10.1126/science.1226340
17. Sundaramurthi D, Rauf S, Hauser C A, 2016, 3D bioprinting technology for regenerative medicine applications. *Int J Bioprint*, 2(2): 117–135. http://dx.doi.org/10.18063/IJB.2016.02.010

18. Hauser C A, Zhang, 2010, Designer self-assembling peptide nanofiber biological materials, 2010, *Chem Soc Rev*, 39(8): 2780–2790. http://dx.doi.org/10.1039/B921448H
19. Loo Y, Zhang S, Hauser C A, 2012, From short peptides to nanofibers to macromolecular assemblies in biomedicine. *Biotechnol Advs*, 30(3): 593–603. http://dx.doi.org/10.1016/j.biotechadv.2011.10.004
20. Wu E C, Zhang S G, Hauser C A E, 2012, Self-assembling peptides as cell-interactive scaffolds. *Adv Funct Mater*, 22(3): 456–468. http://dx.doi.org/10.1002/adfm.201101905
21. Hauser C A, Deng R, Mishra A, *et al*., 2011, Natural tri- to hexapeptides self-assemble in water to amyloid β-type fiber aggregates by unexpected α-helical intermediate structures. *Proceed Natl Acad Sci*, 108(4): 1361–1366. http://dx.doi.org/10.1073/pnas.1014796108
22. Mishra A, Loo Y, Deng R, *et al.*, 2011, Ultrasmall natural peptides self-assemble to strong temperature-resistant helical fibers in scaffolds suitable for tissue engineering. *Nano Today*, 6: 232–239. http://dx.doi.org/10.1016/j.nantod.2011.05.001
23. Reithofer M R, Chan K H, Lakshmanan A, *et al*., 2014, Ligation of anti-cancer drugs to selfassembling ultrashort peptides by click chemistry for localized therapy. *Chem Sci*, 5: 625–630. https://dx.doi.org/10.1039/c3sc51930a
24. Loo Y, Wong Y C, Cai E Z, *et al*., 2014, Ultrashort peptide nanofibrous hydrogels for the acceleration of healing of burn wounds. *Biomaterials*, 35(17): 4805–4814. http://dx.doi.org/10.1016/j.biomaterials.2014.02. 047
25. Kroehne V, Heschel I, Schügner F, *et al*., 2008, Use of a novel collagen matrix with oriented pore structure for muscle cell differentiation in cell culture and in grafts. *J Cell Mol Med*, 12(5a): 1640–1648. http://dx.doi.org/10.1111/j.15824934.2008.00238.x
26. Kang H W, Lee S J, Ko I K, *et al*., 2016, A 3D bioprinting system to produce human-scale tissue constructs with structural integrity. *Nat Biotechnol*, 34(3): 312–319. http://dx.doi.org/10.1038/nbt.3413
27. Chen S, Nakamoto T, Kawazoe N, *et al*., 2015, Engineering multi-layered skeletal muscle tissue by using 3D micro-grooved collagen scaffolds. *Biomaterials*, 73: 23–31. http://dx.doi.org/10.1016/j.biomaterials.2015.09.010
28. Jana S, Cooper A, Zhang M, 2013, Chitosan scaffolds with unidirectional microtubular pores for large skeletal myotube generation. *Adv Healthc Mater*, 2(4): 557–561. https://dx.doi.org/10.1002/adhm.201200177
29. Jana S, Levengood S K L, Zhang M, 2016, Anisotropic materials for skeletal-muscle-tissue engineering. *Adv Mater*, 28(48): 10588–10612. http://dx.doi.org/10.10 02/adma.201600240
30. Koning M, Harmsen M C, Van Luyn M J A, *et al*., 2009, Current opportunities and challenges in skeletal muscle tissue engineering. *J Tissue Eng Regen Med*, 3(6): 407–415. http://dx.doi.org/10.1002/term.190
31. Bian W, Bursac N, 2008, Tissue engineering of functional skeletal muscle: Challenges and recent advances. *IEEE Eng Med Biol Mag*, 27(5): 109–113. http://dx.doi.org/10.1109/MEMB.2008.928460
32. Pollot B E, Rathbone C R, Wenke J C, *et al*., 2017, Natural polymeric hydrogel evaluation for skeletal muscle tissue engineering. *J Biomed Mater Res B Appl Biomater*. http://dx.doi.org/10.1002/jbm.b.33859
33. Loo Y, Lakshmanan A, Ni M, *et al*., 2015, Peptide bioink: Self-assembling nanofibrous scaffolds for three-dimensional organotypic cultures. *Nano Lett*, 15(10): 6919–6925. http://dx.doi.org/10.1021/acs.nanolett.5b02859
34. Taylor S E, Cao T, Talauliker P M, *et al*., 2013, Objective morphological quantification of microscopic images using a fast fourier transform (FFT) analysis. *Curr Protoc Essent Lab Tech*, 7(1):9.5.1–9.5.12. http://dx.doi.org/10.1002/9780470089941.et0905s07
35. Bajaj P, Reddy B Jr, Millet L, *et al*., 2011, Patterning the differentiation of C2C12 skeletal myoblasts. *RSC*, 3(9):897–909. http://dx.doi.org/10.1039/c1ib00058f
36. Matthew D S, Ronald T R, 2010, Collagen structure and stability. *Annu Rev Biochem*, 78: 929–958. https://doi.org/10.1146/annurev.biochem.77.032207.120833
37. Shadrin I Y, Khodabukus A, Bursac N, 2016, Striated muscle function, regeneration, and repair cell. *Mol Life Sci*, 73(22): 4175–4202. http://dx.doi.org/10.1007/s00018-016-2285-z
38. Fuoco C, Petrilli L, Cannata S, *et al*., 2016, Matrix scaffolding for stem cell guidance toward skeletal muscle tissue engineering, *J Orthop Surg Res*, 11: 86. http://dx.doi.org/10.1186/s13018-016-0421-y
39. Fuoco C, Cannata S, Gargioli C, 2016, Could a functional artificial skeletal muscle be useful in muscle wasting? *Curr Opin Clin Nutr Metab Care*, 19(3): 182– 187. http://dx.doi.org/10.1097/MCO.0000000000000 271
40. Mironov V, Kasyanov V, Drake C, *et al*., 2008, Organ printing: Promises and challenges. *Regen Med*, 3(1): 93–103. http://dx.doi.org/10.2217/17460751.3.1.93
41. Choi Y J, Kim T G, Jeong J, *et al*., 2016, 3D cell printing of functional skeletal muscle constructs using skeletal muscle

derived bioink. *Adv Healthc Mater*, 5(20): 2636–2645. http://dx.doi.org/10.1002/adhm. 201600483

42. Fedorovich N E, De Wijn J R, Verbout A J, *et al*., 2008, Three-dimensional fiber deposition of cell-laden, viable, patterned constructs for bone tissue printing. *Tissue Eng Part A*, 14(1): 127–133. http://dx.doi.org/10.1089/ten.a.2007.0158
43. Aviss K J, Gough J E, Downes S, 2010, Aligned electrospun polymer fibres for skeletal muscle regeneration. *Eur Cell Mater*, 19(1): 193–204. http://dx.doi.org/10.22203/eCM. v019a19
44. Macchiarini P, Jungebluth P, Go T, *et al*., 2008, Clinical transplantation of a tissue-engineered airway. *Lancet*, 372(9655): 2023–2030. http://dx.doi.org/10.1016/ S01406736(08)61598-6
45. Martinello T, Bronzini I, Volpin A, *et al*., 2012, Successful recellularization of human tendon scaffolds using adipose-derived mesenchymal stem cells and collagen gel. *J Tissue Eng Regen Med*, 8(8): 612–619. http://dx.doi.org/10.1002/ term.1557
46. Badylak S F, 2004, Xenogeneic extracellular matrix as a scaffold for tissue reconstruction. *Transpl Immunol*, 12(3–4): 367–377. http://dx.doi.org/10.1016/j.trim.2003.12.016
47. Jia J, Richards D J, Pollard S, *et al*., 2014, Engineering alginate as bioink for bioprinting. *Acta Biomater*, 10(10): 4323–4331. http://dx.doi.org/10.1016/j.actbio.2014.06.034
48. Pataky K, Braschler T, Negro A, *et al*., 2012 Microdrop printing of hydrogel bioinks into 3D tissue like geometries. *Adv Mater*, 24(3): 391–396. http://dx.doi.org/10.1002/ adma.201102800
49. Huijun L, Tan Y J, Leong K F, *et al*., 2017, 3D bioprinting of highly thixotropic alginate/methylcellulose hydrogel with strong interface bonding. *ACS Appl Mater Interfaces*, 9(23): 20086–20097. http://dx.doi.org/10.1002/10.1021/ acsami.7b04216
50. Li H, Liu S, Li L, 2016, Rheological study on 3D printability of alginate hydrogel and effect of graphene oxide. *Int J Bioprint*, 2(2): 54–66. http://dx.doi.org/10.18063/ IJB.2016.02.007
51. Luo N C and Grover L M, 2010, Cell encapsulation using biopolymer gels for regenerative medicine. *Biotechnol Lett*, 32(6): 733−742. http://dx.doi.org/10.1007/s10529-010-0221-0
52. Luo K, Yang Y, Shao Z, 2016, Physically crosslinked biocompatible silk-fibroin-based hydrogels with high mechanical performance. *Adv Funct Mater*, 26(6): 872−880. http://dx.doi.org/10.1002/adfm.201503450
53. Kuen Y L, David J M, 2012, Alginate: Properties and biomedical applications, *Prog Polym Sci*, 37(1): 106–126. http://dx.doi.org/10.1016/j.progpolymsci.2011. 06.003
54. Dreesmann L, Ahlers M, Schlosshauer B L, 2007, The pro-angiogenic characteristics of a cross-linked gelatin matrix. *Biomaterials*, 28(36): 5536–5543. http://dx.doi.org/10.1016/ j.biomaterials.2007.0.040
55. Sandrasegaran K, Lall C, Rajesh A, *et al*., 2005, Distinguishing gelatin bioabsorbable sponge and postoperative abdominal abscess on. *Am J Roentgenol*, 184(2): 475–480. http://dx.doi. org/10.2214/ajr.184.2.01840475
56. Balakrishnan B, Mohanty M, Umashankar P R, *et al*., 2005, Evaluation of an *in situ* forming hydrogel wound dressing based on oxidized alginate and gelatin, *Biomaterials*, 26(32), 6335–6342. http://dx.doi.org/10.1016/ j.biomaterials.2005.04.012
57. Rosellini E, Cristallini C, Barbani N, *et al*., 2009, Preparation and characterization of alginate-gelatin blend films for cardiac tissue engineering. *J Biomed Mater Res A*, 91(2): 447–453. http://dx.doi.org/10.1002/jbm.a.32216
58. Dong Z, Wang Q, Du Y, 2006, Blend films and their properties for drug controlled release. *J Memb Sci*, 280(1–2): 37–44. http://dx.doi.org/10.1016/j.memsci. 2006.01.002
59. Fan L, Du L, Huang R, *et al*., 2005, Preparation and characterization of alginate-gelatin blend fibers. *J Appl Polym Sci*, 96(5):1625–1629. http://dx.doi.org/10.1002/ app.21610
60. Li S, Yan Y, Xiong Z, *et al*., 2009, Gradient hydrogel construct based on an improved cell assembling system. *J Bioact Compat Polym*, 24(1): 84–99. http://dx.doi. org/10.1177/0883911509103357
61. Yan Y, Wang X, Xiong Z, 2005, Direct construction of a three-dimensional structure with cells and hydrogel. *J Bioact Compat Polym*, 20(3): 259–269. http://dx.doi. org/10.1177/08839115050536858
62. Li S, Yan Y, Xiong Z, *et al*., 2009, Gradient hydrogel construct based on an improved cell assembling system. *J Bioact Compat Polym*, 24(1): 84–99. http://dx.doi. org/10.1177/0883911509103357
63. Roberto D, Kenneth C H, 2011, Actin structure and function. *Annu Rev Biophys*, 40: 169–186. http://dx.doi. org/10.1146/ annurev-biophys-042910-155359
64. Dado D, Levenberg S, 2009, Cell-scaffold mechanical interplay within engineered tissue. *Semin Cell Dev Biol*, 20(6): 656–664. http:// dx. doi. org/ 10. 1016/ j. semcdb. 2009.02.001

65. Phillips J, Bunting S, Hall S, *et al*., 2005, Neural tissue engineering: A self-organizing collagen guidance conduit. *Tissue Eng*, 11(9–10): 1611–1617. http://dx.doi.org/10. 1089/ten.2005.11.1611

66. Chung C, Bien H, Entcheva E, 2007, The role of cardiac tissue alignment in modulating electrical function. *J Cardiovasc Electrophysiol*, 18(12): 1323– 1329. http://dx.doi.org/10.1111 /j. 15408167. 2007. 009 59.x

67. Zhao Y, Zeng H, Nam J, *et al*., 2009, Fabrication of skeletal muscle constructs by topographic activation of cell alignment. *Biotechnol Bioeng*, 102(2): 624–631. https://doi.org/10.1002/bit.22080

68. Crabb R A, Chau E P, Evans M C, *et al*., 2006, Biomechanical and Microstructural Characteristics of a Collagen Film-Based Corneal Stroma Equivalent, *Tissue Eng*, 12(6): 1565–1575. https://doi.org/10.1089/ten.2006.12.1565

69. Zhu Y, Cao Y, Pan J, *et al*., 2010, Macro-alignment of electrospun fibers for vascular tissue engineering. *J Biomed Mater Res B*, 92(2): 508–516. https://doi.org/10.1002/jbm.b.31544

70. Bajaj P, Khang D and Webster T J, 2006, Control of spatial cell attachment on carbon nanofiber patterns on polycarbonate urethane. *Int J Nanomed*, 1(3): 361–365.